

Hybrid Geomagnetic Attitude and Orbit Estimation Using Time-Differential Feedback*

Jin WU,¹⁾ Chengxi ZHANG,^{2) †} and Ming LIU,¹⁾

¹⁾*Department of Electronic and Computer Engineering, Hong Kong University of Science and Technology, Hong Kong, China*

²⁾*School of Electronic and Information Engineering, Harbin Institute of Technology, Shenzhen, China*

This paper introduces a novel filter for hybrid attitude and orbit estimation of spacecrafts with geomagnetic measurements and its time-differential information. Geomagnetic measurements can be used for simultaneous attitude and orbit estimation of spacecrafts. In practice, the attitude estimation from a single magnetometer is achieved by fusing the magnetometer readings and their time derivatives together. The orbit will also be estimated according to the relationship between the geomagnetic model and spacecraft coordinates in the Earth geodetic frame. However, the magnetic time derivatives have not participated in estimating the orbit elements. According to the mathematical structures of the geomagnetic models, the time-differential feedback can effectively enhance the estimation of the velocity and thus will provide better performance for the position loop. This paper first introduces such direct feedback and formulates a new filter with better characteristics. The simulation study of a medium Earth orbit (MEO) Nadir-pointing satellite mission shows that the proposed filter achieves faster convergence and lower estimation errors.

Key Words: Geomagnetic Measurements, Orbit Determination, Kalman Filter, Time Differential Feedback

1. Introduction

It has been studied recently that multiple sources can be employed for orbit determination, including the visual information, temperature variation and laser scanning measurements.¹⁻³⁾ In fact, most of the spacecrafts will carry magnetometer according to its universality in scientific research and the low costs along with light weight in the study of nanosatellites.⁴⁾ Therefore, the geomagnetic measurements will be applicable to almost any spacecraft for an autonomous orbit determination sub-system. These factors contribute to the reason that magnetometer is often treated as a backup sensor for emerging spacecraft state estimation, subject to a minimum equipment list (MEL).⁵⁾ The dynamical orbit determination problem can be expressed via nonlinear differential systems of the orbit elements. Extensive efforts have been paid to understanding the behaviours of these systems. Also many efficient integrators have been proposed for more accurate orbit propagation.⁶⁾ For the geomagnetic orbit determination, the observation vector can either be the total intensity or the 3-axis components of the measured geomagnetic field. The geomagnetic model can be mathematically described via the spherical harmonic series in terms of the local geodetic coordinates. As the geomagnetic model is expressed in the geodetic frame, 3-axis measurements require attitude information of the spacecraft, which is not needed by the total intensity due to the norm invariance of the rotation.⁷⁾ As the magnetometer also reflects the attitude information,^{8,9)} it is feasible that the attitude and orbit can be simultaneously estimated via a single magnetometer.¹⁰⁾ Dated back to the late

1980s, the geomagnetic orbit determination method was first studied by Psiaki et al.¹¹⁾ Due to high nonlinearity of the global geomagnetic model and large magnetic uncertainty of the instruments, the orbit determination accuracy is not so satisfactory. This was then resolved by introducing external sources like Sun sensor and star tracker.^{12,13)} However, as the magnetometer is quite flexible, the researchers have always been continuously working on more effective estimation approaches during the past several decades. Juang et al. applied the magnetometer dynamic calibration to the geomagnetic orbit determination and achieved better accuracy.¹⁴⁾ Cheon has proposed a method for target pointing spacecraft that the included angle between the magnetic vector and the pointing vector can be used for enhanced geomagnetic orbit determination.¹⁵⁾ It is also shown that combining with multiple sensors, the spacecraft navigation performance can be improved.¹⁶⁾

Using filtering techniques like extended Kalman filter (EKF) and unscented Kalman filter (UKF), it is proven that drift-free orbit determination can be performed. Although existing works have shown current feasibility of geomagnetic orbit determination, a drawback still consists in the conventional model that there is no direct velocity feedback in the observation model so that the filter typically requires a few hours or more to converge to a satisfactory estimate.¹⁵⁾ This paper introduces the time-differential information as the direct velocity feedback to the simultaneous geomagnetic attitude and orbit estimation for the very first time. The aim of this study is to show that such feedback will be efficient. It is investigated that the closed forms of the time-differential model can be obtained. A new filter design has been proposed for better estimation performance on the convergence and accuracy.

The remainder of this paper is organized as follows: Section II contains the proposed geomagnetic attitude and orbit

© 2020 The Japan Society for Aeronautical and Space Sciences

*Received X X 20XX; final revision received X X 20XX; accepted for publication X X 20XX

†Corresponding author, dongfangxy@163.com

estimation filter design. Section III presents the simulation results and the concluding remarks have been drawn in Section IV.

2. Time-Differential Geomagnetic Model

The magnetometer mounted on the spacecraft measures the geomagnetic field \mathbf{B}^b in the body frame b . According to the attitude dynamics, the geomagnetic measurement and its time derivative can be related as follows⁴⁾

$$\begin{cases} \mathbf{B}^b = \mathbf{R}_{\text{NED}}^b \mathbf{B}^{\text{NED}} \\ \dot{\mathbf{B}}^b = \mathbf{R}_{\text{NED}}^b \dot{\mathbf{B}}^{\text{NED}} - \boldsymbol{\omega} \times (\mathbf{R}_{\text{NED}}^b \mathbf{B}^{\text{NED}}) \end{cases} \quad (1)$$

where \mathbf{B}^{NED} denotes the geomagnetic reference vector in the local North-East-Down (NED) frame and $\mathbf{R}_{\text{NED}}^b$ defines a transformation matrix from NED frame to the b frame. $\boldsymbol{\omega}$ represents the angular rate vector of the spacecraft body with respect to the reference frame. The spacecraft attitude dynamics follow that¹⁷⁾

$$\dot{\boldsymbol{\omega}} = -\mathbf{I}^{-1} [\boldsymbol{\omega} \times (\mathbf{I}\boldsymbol{\omega} + \mathbf{u})] + \mathbf{I}^{-1} (\mathbf{T} - \dot{\mathbf{u}}) \quad (2)$$

with \mathbf{I} the inertia matrix, \mathbf{u} the angular momentum of the reaction wheel and \mathbf{T} the external torques imposed on the spacecraft, including the aerodynamic drag, geopotential gradient, equivalent magnetic disturbance torque from spaceborne currents and etc. Abdelrahman et al. employ (1) as the observation model for the simultaneous attitude and orbit determination by setting an augmented dynamics extended Kalman filter (ADEKF) with a state vector incorporating angular rate, quaternion, position, velocity and drag coefficient.⁷⁾ It has been proven to be efficient in real missions due to the fact that at least two vector measurements guarantee the observability of full attitude of $\mathbf{R}_{\text{NED}}^b$. One current drawback of their method is that the time derivatives of the geomagnetic measurements in both body and reference frames are computed via the polynomial extrapolation. That is to say, in their observation model, both $\dot{\mathbf{B}}^b$ and $\dot{\mathbf{B}}^{\text{NED}}$ are computed from historical measurements. Therefore, there is no direct or indirect differential feedback to the attitude and orbit. Thus the orbital convergence of the ADEKF subject to large initial state bias, will be slow. Besides, the model (1) does not consider the time-varying magnetometer disturbance that may severely impact the navigation performance.

The magnetometer model can be further revised to

$$\mathbf{B}^b = \mathbf{R}_{\text{NED}}^b \mathbf{B}^{\text{NED}} + \mathbf{b} + \boldsymbol{\eta} \quad (3)$$

where \mathbf{b} and $\boldsymbol{\eta}$ are the dynamical disturbance and the additive noise item subject to the Gaussian distribution $\boldsymbol{\eta} \sim \mathcal{N}(\bar{\boldsymbol{\eta}}, \boldsymbol{\Sigma}_{\boldsymbol{\eta}})$ with $\bar{\boldsymbol{\eta}}$ the mean value and $\boldsymbol{\Sigma}_{\boldsymbol{\eta}}$ the covariance matrix. Soken et al. have recently proposed an attitude-independent observation model for estimation of \mathbf{b} :¹⁸⁾

$$\|\mathbf{B}^b\|^2 - \|\mathbf{B}^{\text{NED}}\|^2 = 2\mathbf{B}^b \cdot \mathbf{b} - \|\mathbf{b}\|^2 + \xi \quad (4)$$

where

$$\xi = 2(\mathbf{B}^b - \mathbf{b}) \cdot \boldsymbol{\eta} \quad (5)$$

subject to the Gaussian distribution such that

$$\xi \sim \mathcal{N} \left[-\text{tr} \boldsymbol{\Sigma}_{\boldsymbol{\eta}}, 4(\mathbf{B}^b - \mathbf{b})^\top \boldsymbol{\Sigma}_{\boldsymbol{\eta}} (\mathbf{B}^b - \mathbf{b}) + 2\text{tr} \boldsymbol{\Sigma}_{\boldsymbol{\eta}} \right] \quad (6)$$

In Soken's work,¹⁸⁾ $\dot{\mathbf{b}} = \mathbf{0}$ has been assumed as the system model of \mathbf{b} . However, for fast varying magnetic disturbances like those caused by geomagnetic storms, this constant assumption will no longer be feasible. Differentiating (3) in terms of the time gives

$$\begin{aligned} \dot{\mathbf{B}}^b &= \mathbf{R}_{\text{NED}}^b \dot{\mathbf{B}}^{\text{NED}} - \boldsymbol{\omega} \times (\mathbf{R}_{\text{NED}}^b \mathbf{B}^{\text{NED}}) + \dot{\mathbf{b}} + \dot{\boldsymbol{\eta}} \\ \Rightarrow \dot{\mathbf{b}} &= \boldsymbol{\omega} \times (\mathbf{R}_{\text{NED}}^b \mathbf{B}^{\text{NED}}) - \mathbf{R}_{\text{NED}}^b \dot{\mathbf{B}}^{\text{NED}} - \dot{\mathbf{B}}^b - \dot{\boldsymbol{\eta}} \end{aligned} \quad (7)$$

which can be used as the dynamical system model of \mathbf{b} . What needs to be point out is that here the system model of \mathbf{b} is no longer attitude-free.

The internal reason that (1) can estimate the orbit is that \mathbf{B}^{NED} is a function of the geodetic coordinates r, θ, φ , namely, the radial distance to the center of the Earth, the co-elevation and the latitude. The geomagnetic potential at one point is given by spherical harmonic series

$$\begin{aligned} V(r, \theta, \varphi, l) &= \\ R_e \sum_{n=1}^q \left(\frac{R_e}{r} \right)^{n+1} \sum_{m=0}^n (g_n^m \cos m\varphi + h_n^m \sin m\varphi) P_n^m(\cos \theta) \end{aligned} \quad (8)$$

where $P_n^m(\cos \theta)$ denotes the Schmidt associated Legendre function with degrees n and m up to l that is orthogonal on a sphere; g_n^m and h_n^m are required Gaussian coefficients which have been extensively studied via historical geomagnetism observations. The International Geomagnetic Reference Field (IGRF), the Enhanced Magnetic Model (EMM) and the World Magnetic Model (WMM) are all based on the same geopotential $V(r, \theta, \varphi, l)$ with different values of g_n^m and h_n^m . Theoretical spherical harmonic analysis have proven that the geomagnetic vector in the NED reference frame is the solution to the Laplacian equation $\nabla^2 V(r, \theta, \varphi, l) = 0$, i.e.

$$\mathbf{B}^{\text{NED}} = -\nabla V(r, \theta, \varphi, l) = (B_r, B_\theta, B_\varphi)^\top \quad (9)$$

which yields

$$\begin{aligned} B_r &= \\ &\sum_{n=1}^l \left(\frac{R_e}{r} \right)^{n+2} (n+1) \sum_{m=0}^n (g_n^m \cos m\varphi + h_n^m \sin m\varphi) P_n^m(\cos \theta) \\ B_\theta &= - \sum_{n=1}^l \left(\frac{R_e}{r} \right)^{n+2} \sum_{m=0}^n (g_n^m \cos m\varphi + h_n^m \sin m\varphi) \frac{\partial P_n^m(\cos \theta)}{\partial \theta} \\ B_\varphi &= \\ &-\frac{1}{\sin \theta} \sum_{n=1}^l \left(\frac{R_e}{r} \right)^{n+2} \sum_{m=0}^n m (-g_n^m \sin m\varphi + h_n^m \cos m\varphi) P_n^m(\cos \theta) \end{aligned} \quad (10)$$

To decrease the shortcomings of the filters by Abdelrahman et al., the following filter framework is proposed:

- State Vector:** The state vector includes the angular rate $\boldsymbol{\omega}$, rotation vector $\boldsymbol{\phi}$ parameterizing the rotation matrix $\mathbf{R}_{\text{NED}}^b$, orbit position \mathbf{p}_{ECI} , orbiting velocity \mathbf{v}_{ECI} in the Earth centered inertial (ECI) frame and the magnetometer disturbance \mathbf{b} so that the state can be represented in the form of

$$\mathbf{x} = (\boldsymbol{\omega}^\top, \boldsymbol{\phi}^\top, \mathbf{p}_{\text{ECI}}^\top, \mathbf{v}_{\text{ECI}}^\top, \mathbf{b}^\top)^\top \quad (11)$$

2. Process Model:

(a) **Angular Dynamics:** The equation in (2).

(b) **Quaternion Dynamics:**

$$\dot{\phi} = \omega + \frac{1}{2}\phi \times \omega + \frac{1}{12}\phi \times (\phi \times \omega) \quad (12)$$

where the coning correction is considered.¹⁹⁾

(c) **Position and Velocity:**

$$\begin{cases} \dot{p}_{\text{ECI}} = v_{\text{ECI}} \\ \dot{v}_{\text{ECI}} = a_{\text{dyn}} + a_{\text{ext}} \end{cases} \quad (13)$$

where a_{dyn} represents the geopotential dynamical acceleration while a_{ext} describes all the external disturbance accelerations, including atmospheric drag, solar radiation pressure, Sun/Moon gravitational forces and etc. In this paper, the the gravity model with items up to J_4 has been employed, which is as a_{dyn} shown in (26) in the appendix. For a_{ext} , the atmospheric drag is neglected according to relatively high altitude of the flight trajectory.

(d) **Magnetic Disturbance:** The equation in (7).

3. **Observation Model:** The measurement vector is

$$z = \left[(B^b)^\top, (\dot{B}^b)^\top, \|\dot{B}^b\|^2, \|B^b\|^2 - \|B^{\text{NED}}\|^2 \right]^\top \quad (14)$$

where B^b and \dot{B}^b are three-axis geomagnetic measurement and its time derivative in the spacecraft body frame; $\|B^{\text{NED}}\|$ is the total intensity of the magnetometer and may usually derived from the scalar magnetometer; The squared norm of the \dot{B}^b follows that

$$\begin{aligned} \|\dot{B}^b\|^2 &= \left[R_{\text{NED}}^b \dot{B}^{\text{NED}} - \omega \times (R_{\text{NED}}^b B^{\text{NED}}) \right]^\top \\ &\quad \left[R_{\text{NED}}^b \dot{B}^{\text{NED}} - \omega \times (R_{\text{NED}}^b B^{\text{NED}}) \right] \\ &= \|\dot{B}^{\text{NED}}\|^2 + \|\omega\|^2 \|B^{\text{NED}}\|^2 - \\ &\quad 2(R_{\text{NED}}^b \dot{B}^{\text{NED}}) \cdot [\omega \times (R_{\text{NED}}^b B^{\text{NED}})] \end{aligned} \quad (15)$$

It can be seen that when $\|\omega\|^2$ is a tiny number, denoting that the angular rate with respect to the NED frame is tiny, such as the Nadir alignment attitude profile, the main factor in \dot{B}^b will be $\|\dot{B}^{\text{NED}}\|^2$. The measurement of \dot{B}^b also comes from the scalar magnetometer and one may observe in (15) that $\|\dot{B}^b\|^2$ is dependent on the time derivative of B^{NED} , which can be given by (16). $\|B^b\|$ provides the direct observability of the position p_{ECI} while $\|\dot{B}^b\|^2$ gives the feedback of the velocity from $\dot{r}, \dot{\theta}, \dot{\varphi}$. The values of $\dot{r}, \dot{\theta}, \dot{\varphi}$ are converted using predicted velocity from the ECI coordination system to the local geodetic NED frame. Such detailed transformations can be found in²⁰⁾ paper that such transformation from the Cartesian ECI frame to the geodetic spherical frame in the way of closed-forms does not always guarantee the least transformation errors and further optimization techniques are required to decrease such effect.²¹⁾

The final item in z considers the magnetic disturbance estimation, which has been presented in (4). It can be

inferred from this term that the magnetometer calibration model also contributes to the estimation of the orbit elements. The designed structure of z therefore consists of full observability of attitude, orbit and magnetometer disturbance and will own higher accuracy and faster convergence speed upon implementation.

$$\begin{aligned} \dot{B}_r &= -\frac{1}{R_e} \sum_{n=1}^q \dot{r} \left(\frac{R_e}{r} \right)^{n+3} (n+1)(n+2) \times \\ &\quad \sum_{m=0}^n (g_n^m \cos m\varphi + h_n^m \sin m\varphi) P_n^m(\cos \theta) + \\ &\quad \sum_{n=1}^q \left(\frac{R_e}{r} \right)^{n+2} (n+1) \times \\ &\quad \sum_{m=0}^n \left[\begin{array}{l} m \left(\begin{array}{l} -g_n^m \dot{\varphi} \sin m\varphi + \\ h_n^m \dot{\varphi} \cos m\varphi \end{array} \right) P_n^m(\cos \theta) + \\ \left(\begin{array}{l} g_n^m \cos m\varphi + \\ h_n^m \sin m\varphi \end{array} \right) \dot{P}_n^m(\cos \theta) \end{array} \right] \end{aligned} \quad (16a)$$

$$\begin{aligned} \dot{B}_\theta &= \frac{1}{R_e} \sum_{n=1}^q \dot{r} \left(\frac{R_e}{r} \right)^{n+3} (n+2) \times \\ &\quad \sum_{m=0}^n (g_n^m \cos m\varphi + h_n^m \sin m\varphi) \frac{\partial P_n^m(\cos \theta)}{\partial \theta} - \\ &\quad \sum_{n=1}^q \left(\frac{R_e}{r} \right)^{n+2} \sum_{m=0}^n \left[\begin{array}{l} m \left(\begin{array}{l} -g_n^m \dot{\varphi} \sin m\varphi + \\ h_n^m \dot{\varphi} \cos m\varphi \end{array} \right) \frac{\partial P_n^m(\cos \theta)}{\partial \theta} + \\ \left(\begin{array}{l} g_n^m \cos m\varphi + \\ h_n^m \sin m\varphi \end{array} \right) \frac{\partial^2 P_n^m(\cos \theta)}{\partial \theta \partial t} \end{array} \right] \end{aligned} \quad (16b)$$

$$\begin{aligned} \dot{B}_\varphi &= -\dot{\theta} \cot \theta B_\varphi + \\ &\quad \frac{1}{R_e \sin \theta} \sum_{n=1}^q \dot{r} \left(\frac{R_e}{r} \right)^{n+3} (n+2) \times \\ &\quad \sum_{m=0}^n m (-g_n^m \sin m\varphi + h_n^m \cos m\varphi) P_n^m(\cos \theta) - \\ &\quad \frac{1}{\sin \theta} \sum_{n=1}^q \left(\frac{R_e}{r} \right)^{n+2} \times \\ &\quad \sum_{m=0}^n \left[\begin{array}{l} -m^2 \left(\begin{array}{l} g_n^m \dot{\theta} \cos m\varphi + \\ h_n^m \dot{\theta} \sin m\varphi \end{array} \right) P_n^m(\cos \theta) + \\ m \left(\begin{array}{l} -g_n^m \sin m\varphi + \\ h_n^m \cos m\varphi \end{array} \right) \dot{P}_n^m(\cos \theta) \end{array} \right] \end{aligned} \quad (16c)$$

with derivatives of Legendre functions as follows

$$\begin{aligned} \dot{P}_n^m(\cos \theta) &= \frac{\partial P_n^m(\cos \theta)}{\partial \theta} \dot{\theta} \\ \frac{\partial^2 P_n^m(\cos \theta)}{\partial \theta \partial t} &= \frac{\partial^2 P_n^m(\cos \theta)}{\partial \theta^2} \dot{\theta} \end{aligned} \quad (17)$$

where

$$\begin{aligned}
 \frac{\partial^2 P_0^0(\cos \theta)}{\partial \theta^2} &= 0 \\
 \frac{\partial^2 P_n^n(\cos \theta)}{\partial \theta^2} &= \cos \theta \frac{\partial^2 P_{n-1}^{n-1}(\cos \theta)}{\partial \theta^2} - \sin \theta \frac{\partial P_{n-1}^{n-1}(\cos \theta)}{\partial \theta} \\
 &\quad - \sin \theta \frac{\partial P_{n-1}^{n-1}(\cos \theta)}{\partial \theta} - \cos \theta P_{n-1}^{n-1}(\cos \theta) \quad , n \geq 1 \\
 \frac{\partial^2 P_n^m(\cos \theta)}{\partial \theta^2} &= \cos \theta \frac{\partial^2 P_{n-1}^m(\cos \theta)}{\partial \theta^2} - \sin \theta \frac{\partial P_{n-1}^m(\cos \theta)}{\partial \theta} \\
 &\quad - \sin \theta \frac{\partial P_{n-1}^m(\cos \theta)}{\partial \theta} - \cos \theta P_{n-1}^m(\cos \theta) \\
 &\quad - K_n^m \frac{\partial^2 P_{n-2}^m(\cos \theta)}{\partial \theta^2}
 \end{aligned} \tag{18}$$

In,^{4,7)} the time derivatives of the geomagnetic measurements are computed from \mathbf{B}^b using the polynomial extrapolation. The method is practical but lacks in estimating accurate covariance. We hereby introduce the window-recursive approach (WRA) for estimation of the derivatives.²²⁾ WRA technique has been successfully applied to the estimation of GNSS real-time kinematic velocity model and can reach to arbitrary order using historical data.^{23,24)} An alternative advantage of the WRA is that it can give accurate covariance results of the estimates, which has not been considered in the previous polynomial interpolation based methods.^{4,5)} In this work, it is assumed that $d\dot{\mathbf{B}}^b/dt = \mathbf{0}$, so the WRA owns the second order.

3. Simulation Results

As the orbit propagation presented in the state process model neglects the external acceleration from atmospheric drag, in this section, a mission of the medium Earth orbit (MEO) satellite has been simulated. The Earth-orbiting mission has been simulated with eccentricity of 0.15 and semi-major axis of 9966.14 km. The equivalent orbit parameters in the J2000 ECI frame are

$$\begin{aligned}
 \mathbf{p}_{\text{ECI}} &= \begin{pmatrix} 6293.3980673746755201 \\ 2770.2470960305845438 \\ -11.4819540016413821 \end{pmatrix} \text{ km} \\
 \mathbf{v}_{\text{ECI}} &= \begin{pmatrix} -2.1591063642755022 \\ 4.9273503592517010 \\ 5.3877766489578649 \end{pmatrix} \text{ km/s}
 \end{aligned} \tag{19}$$

The satellite attitude profile is set as Nadir alignment subject to orbit normal constraint of 3 deg. The spacecraft weighs at 1000kg and owns the inertia matrix of $\mathbf{I} = \text{diag}(4500, 4500, 4500) \text{ kg} \cdot \text{m}^2$. A 3-axis magnetometer and an independent scalar magnetometer have been installed on the satellite with 1σ measurement uncertainties of 2 nT and 0.5 nT respectively. The outer geomagnetic environment is perturbed with the Olson-Pfitzer field.²⁵⁾ The space weather has been simulated according to the NASA online profiles. A scenario with time span of 24 hours is created. The attitude control method used in this paper is based on a proportional-derivative (PD) design. The estimation problem can be ex-

pressed via the solution to the following system

$$\begin{cases} \dot{\mathbf{x}} = \mathbf{f}(\mathbf{x}, t) + \boldsymbol{\kappa} \\ \mathbf{z} = \mathbf{h}(\mathbf{x}, t) + \boldsymbol{\varrho} \end{cases} \tag{20}$$

where $\mathbf{f}(\mathbf{x}, t)$ and $\mathbf{h}(\mathbf{x}, t)$ define the process and observation models respectively, with respect to the state \mathbf{x} and time t ; $\boldsymbol{\kappa}$ and $\boldsymbol{\varrho}$ are additive noise items whose online uncertainties (covariance) $\boldsymbol{\Sigma}_{\boldsymbol{\kappa}}$ and $\boldsymbol{\Sigma}_{\boldsymbol{\varrho}}$ can be evaluated using either the first-order approximation or the method of sigma points. Representative methods utilize the EKF and UKF for state estimation. However, in the proposed models, due to the fact that the internal variables and their uncertainty descriptions are deeply coupled and correlated, in the simulation study, the state-dependent Riccati equation (SDRE) filtering has been invoked to avoid the non-optimality of the EKF and UKF. The SDRE first seeks a model that approximates (20) by

$$\begin{cases} \dot{\hat{\mathbf{x}}} = \mathbf{F}(\hat{\mathbf{x}})\hat{\mathbf{x}} + \boldsymbol{\kappa} \\ \mathbf{z} = \mathbf{H}(\hat{\mathbf{x}})\hat{\mathbf{x}} + \boldsymbol{\varrho} \end{cases} \tag{21}$$

where \mathbf{F} and \mathbf{H} can typically be obtained via Jacobians of \mathbf{f} and \mathbf{h} at the latest estimate $\hat{\mathbf{x}}$. The correction update of the SDRE filtering about the estimated state $\hat{\mathbf{x}}$ is given by

$$\hat{\mathbf{x}} = \mathbf{F}(\hat{\mathbf{x}})\hat{\mathbf{x}} + \mathbf{K}[\mathbf{z} - \mathbf{H}(\hat{\mathbf{x}})\hat{\mathbf{x}}] \tag{22}$$

with \mathbf{K} being the feedback gain matrix subject to the following linear design

$$\mathbf{K} = \mathbf{P}\mathbf{H}^T(\hat{\mathbf{x}})\boldsymbol{\Sigma}_{\boldsymbol{\varrho}} \tag{23}$$

where \mathbf{P} is the symmetric positive semidefinite solution to the continuous algebraic Riccati equation (CARE) such that

$$\mathbf{F}(\hat{\mathbf{x}})\mathbf{P} + \mathbf{P}\mathbf{F}^T(\hat{\mathbf{x}}) - \mathbf{P}\mathbf{H}^T(\hat{\mathbf{x}})\boldsymbol{\Sigma}_{\boldsymbol{\varrho}}^{-1}\mathbf{H}(\hat{\mathbf{x}})\mathbf{P} + \boldsymbol{\Sigma}_{\boldsymbol{\kappa}} = \mathbf{0} \tag{24}$$

The total intensity difference between the IGRF model of degree 12 and the measured magnitude from the spacecraft body frame using scalar magnetometer is shown in Fig. 2. It can be seen that due to the space time-varying high-energy flux and external geomagnetic field, the difference can reach up to 150 nT. Such mismatch can actually be characterized as the outer magnetic disturbance, which will be estimated in the following contents. As the attitude propagates subject to the Nadir alignment, $\|\boldsymbol{\omega}\|^2$ are quite small. Therefore $\|\dot{\mathbf{B}}^{\text{NED}}\|^2$ is the major contribution to $\|\dot{\mathbf{B}}^b\|^2$ according to (7). The time derivatives of the geomagnetic total intensity from the simulated NED frame and that from the measured vectors in the body frame can be observed in Fig. 3. The shown values indicates such trend and prove that this type of measurement will be feasible for orbit determination.

Using the simulated data and the PD control method, the spacecraft attitude/orbit estimation is conducted. The estimation frequency has been set to 1Hz which is quite enough for spacecraft state estimation and control. The initial position bias has been set to 1×10^3 km and the initial velocity bias is 1 km/s. The initial angular rate and the rotation vector are set to $\boldsymbol{\omega} = \boldsymbol{\phi} = \mathbf{0}$. The initial magnetic disturbance is also zero that will be estimated in further updates. To be consistent with previous Abdelrahman's ADEKF,⁷⁾ the estimated

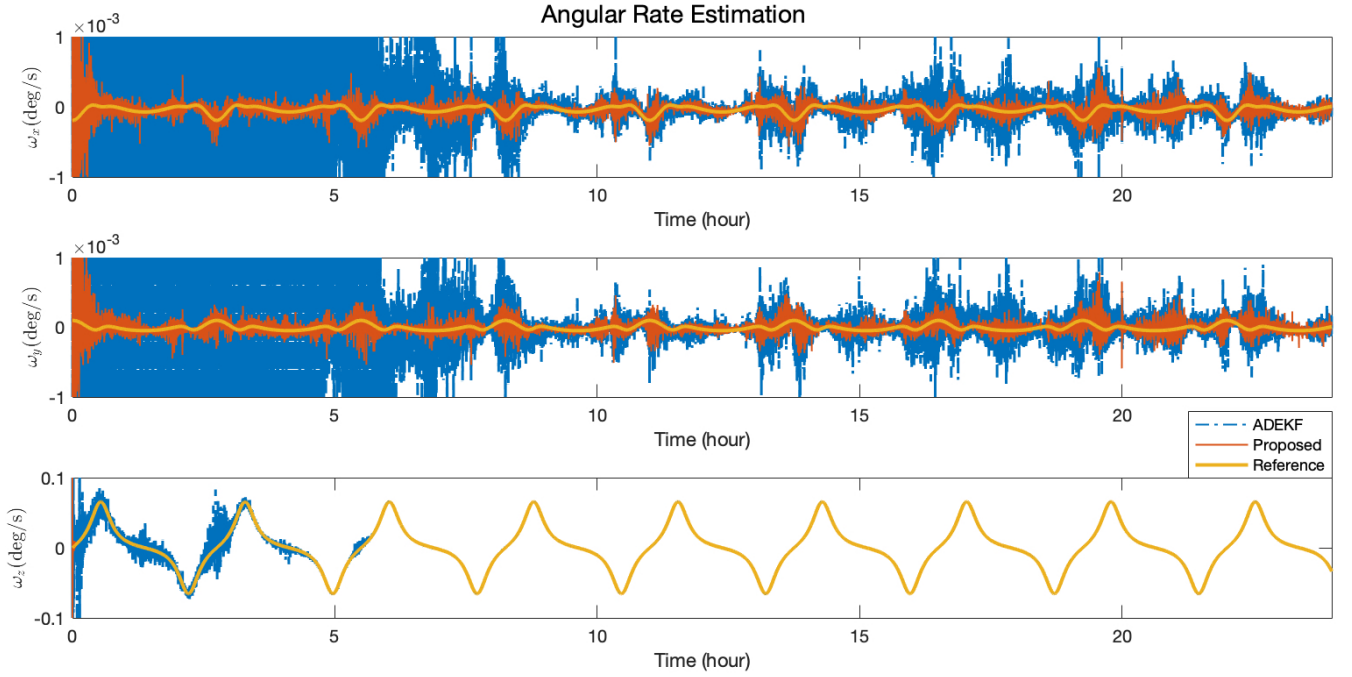


Fig. 1. The estimated angular rate vectors.

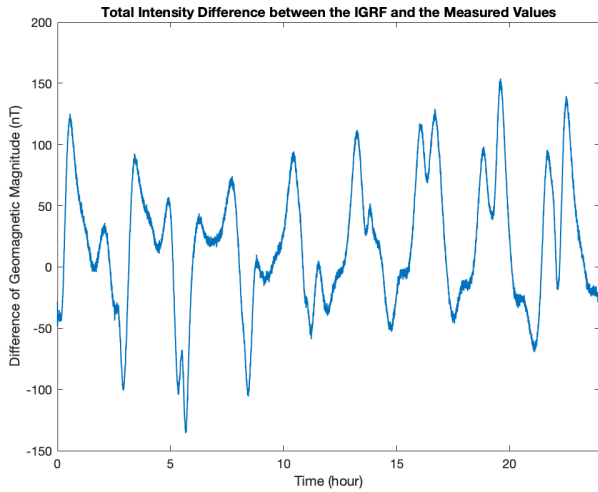


Fig. 2. The total intensity difference between the 12-th IGRF model and the measured magnitude.

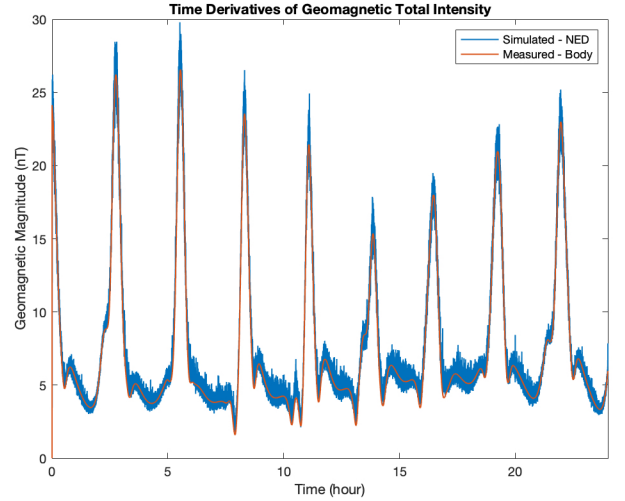


Fig. 3. The time derivatives of the geomagnetic total intensity in various frames.

rotation vector ϕ is cast into the form of unit quaternion such that²⁶⁾

$$\mathbf{q} = \left(\cos \frac{\|\phi\|}{2}, \sin \frac{\|\phi\|}{2} \phi^\top \right)^\top \quad (25)$$

paper that both \mathbf{q} and $-\mathbf{q}$ represent the same rotation matrix, then the post processing for sign ambiguity has been performed according to.²⁷⁾ The estimated angular rate and the quaternion along with the quaternion errors are shown in Fig. 1 and 4 respectively. One can see that due to the cancellation of the magnetic disturbance, which is shown in Fig. 5, the estimation results have been more accurate compared with the ADEKF. By virtue of the time-differential feedback, there are now two direct sources for orbit determination and thus the convergence of the filter has been significantly improved. The position and velocity estimation results are presented in the form of errors by Fig. 6. It is evident that the initial converging rate of the proposed filter is much higher than that

of the ADEKF. Besides, due to the introduction of direct differential feedback, the observability of the velocity has been enhanced and both the position and velocity errors have been decreased.

4. Conclusion

The geomagnetic attitude/orbit estimation problem has been revisited. It is shown that time-differential information of the geomagnetic field model will benefit the estimation convergence and accuracy. However, it is worth noting that the new filter incorporates higher dimension of the observation model and will require computation of the derivatives of the IGRF model. Therefore, the computational efficiency of the proposed algorithms will be obviously worse than some previous representatives.

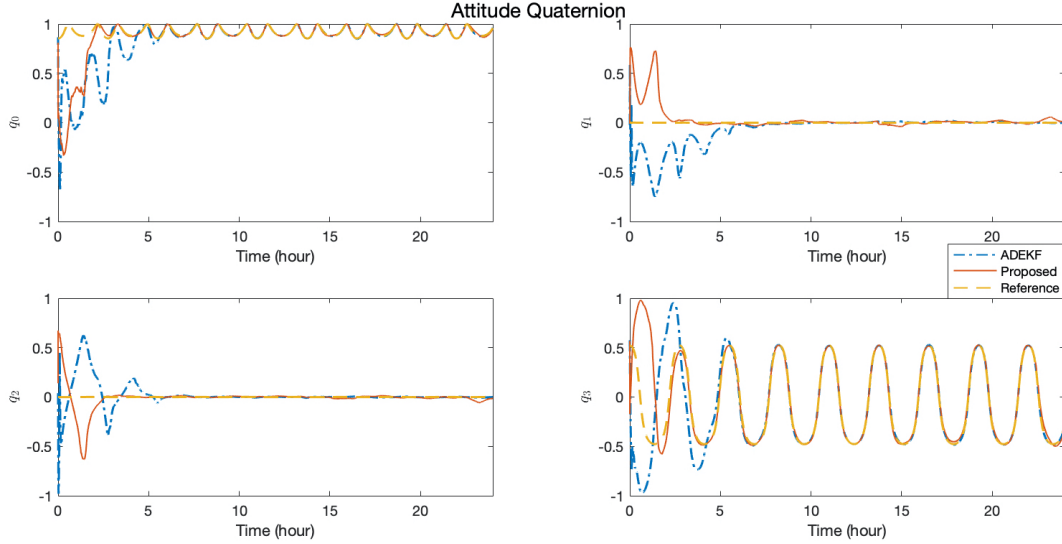


Fig. 4. Estimated quaternions from different sources.

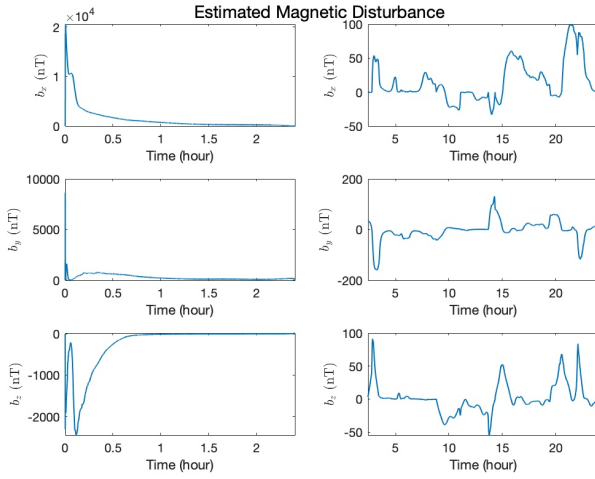


Fig. 5. The estimated magnetic disturbance.

Appendix: J_4 Geopotential Model

The J_4 -perturbed geopotential model is

$$\begin{aligned} \mathbf{a}_{\text{dyn}} &= (a_{\text{ECL},x}, a_{\text{ECL},y}, a_{\text{ECL},z})^\top \\ a_{\text{ECL},x} &= -\frac{\mu p_{\text{ECL},x}}{r^3} \times \\ &\quad \left[\begin{array}{l} 1 + \frac{3}{2} J_2 \left(\frac{R_e}{r} \right)^2 \left(1 - 5 \frac{p_{\text{ECL},z}^2}{r^2} \right) \\ + \frac{5}{2} J_3 \left(\frac{R_e}{r} \right)^3 \left(3 \frac{p_{\text{ECL},z}}{r} - 7 \frac{p_{\text{ECL},z}^3}{r^3} \right) \\ - \frac{5}{8} J_4 \left(\frac{R_e}{r} \right)^4 \left(3 - 42 \frac{p_{\text{ECL},z}^2}{r^2} + 63 \frac{p_{\text{ECL},z}^4}{r^4} \right) \end{array} \right] \\ a_{\text{ECL},y} &= -\frac{\mu p_{\text{ECL},y}}{r^3} \times \\ &\quad \left[\begin{array}{l} 1 + \frac{3}{2} J_2 \left(\frac{R_e}{r} \right)^2 \left(1 - 5 \frac{p_{\text{ECL},z}^2}{r^2} \right) \\ + \frac{5}{2} J_3 \left(\frac{R_e}{r} \right)^3 \left(3 \frac{p_{\text{ECL},z}}{r} - 7 \frac{p_{\text{ECL},z}^3}{r^3} \right) \\ - \frac{5}{8} J_4 \left(\frac{R_e}{r} \right)^4 \left(3 - 42 \frac{p_{\text{ECL},z}^2}{r^2} + 63 \frac{p_{\text{ECL},z}^4}{r^4} \right) \end{array} \right] \end{aligned} \quad (26a)$$

$$\begin{aligned} a_{\text{ECL},z} &= -\frac{\mu p_{\text{ECL},x}}{r^3} \times \\ &\quad \left[\begin{array}{l} 1 + \frac{3}{2} J_2 \left(\frac{R_e}{r} \right)^2 \left(3 - 5 \frac{p_{\text{ECL},z}^2}{r^2} \right) \\ + \frac{5}{2} J_3 \left(\frac{R_e}{r} \right)^3 \left(6 \frac{p_{\text{ECL},z}}{r} - 7 \frac{p_{\text{ECL},z}^3}{r^3} - \frac{3r}{5 p_{\text{ECL},z}} \right) \\ - \frac{5}{8} J_4 \left(\frac{R_e}{r} \right)^4 \left(15 - 70 \frac{p_{\text{ECL},z}^2}{r^2} + 63 \frac{p_{\text{ECL},z}^4}{r^4} \right) \end{array} \right] \end{aligned} \quad (26b)$$

where $p_{\text{ECL}} = (p_{\text{ECL},x}, p_{\text{ECL},y}, p_{\text{ECL},z})^\top$ is the position in the ECI frame, μ is the gravitational constant of the Earth, J_2, J_3 and J_4 are zonal constant of the gravitational field.

References

- 1) Gu, L., Jiang, X., Li, S., and Li, W.: Optical/Radio/Pulsars Integrated Navigation for Mars Orbiter, *Adv. Space Res.*, **63**, 1, 2018, pp. 512–525.
- 2) Nasihati Gourabi, F., Kiani, M., and Pourtakdoust, S. H., “Autonomous Temperature-Based Orbit Estimation,” *Aerosp. Sci. Tech.*, **86**, 2019, pp. 671–682.
- 3) Psiaki, M. L.: Laser Ranging To Unknown Objects for Initial Orbit Determination: A Feasibility Study, *AIAA J. Guid. Control Dyn.*, 2019.
- 4) Abdelrahman, M., and Park, S. Y.: Sigma-Point Kalman Filtering for Spacecraft Attitude and Rate Estimation using Magnetometer Measurements, *IEEE Trans. Aerosp. Elect. Syst.*, **47**, 2, 2011a, pp. 1401–1415.
- 5) Abdelrahman, M., and Park, S. Y.: Integrated Attitude Determination and Control System via Magnetic Measurements and Actuation, *Acta Astronaut.*, **69**, 3-4, 2011b, pp. 168–185.
- 6) Woollands, R. M., Bani Younes, A., and Junkins, J. L.: New Solutions for the Perturbed Lambert Problem Using Regularization and Picard Iteration, *AIAA J. Guid. Control Dyn.*, **38**, 9, 2015, pp. 1548–1562.
- 7) Abdelrahman, M., and Park, S. Y.: Simultaneous Spacecraft Attitude and Orbit Estimation using Magnetic Field Vector Measurements, *Aerosp. Sci. Tech.*, **15**, 8, 2011c, pp. 653–669.
- 8) Ahn, H. S., and Lee, S. H.: Gyroless Attitude Estimation of Sun-Pointing Satellites using Magnetometers, *IEEE Geosci. Remote Sens. Lett.*, **2**, 1, 2005, pp. 8–12.
- 9) Roberts, T. M., Lynch, K. A., Clayton, R. E., Disbrow, M. E., and Hansen, C. J.: Magnetometer-Based Attitude Determination for Deployed Spin-Stabilized Spacecraft, *AIAA J. Guid. Control Dyn.*, **40**, 11, 2017, pp. 2941–2947.

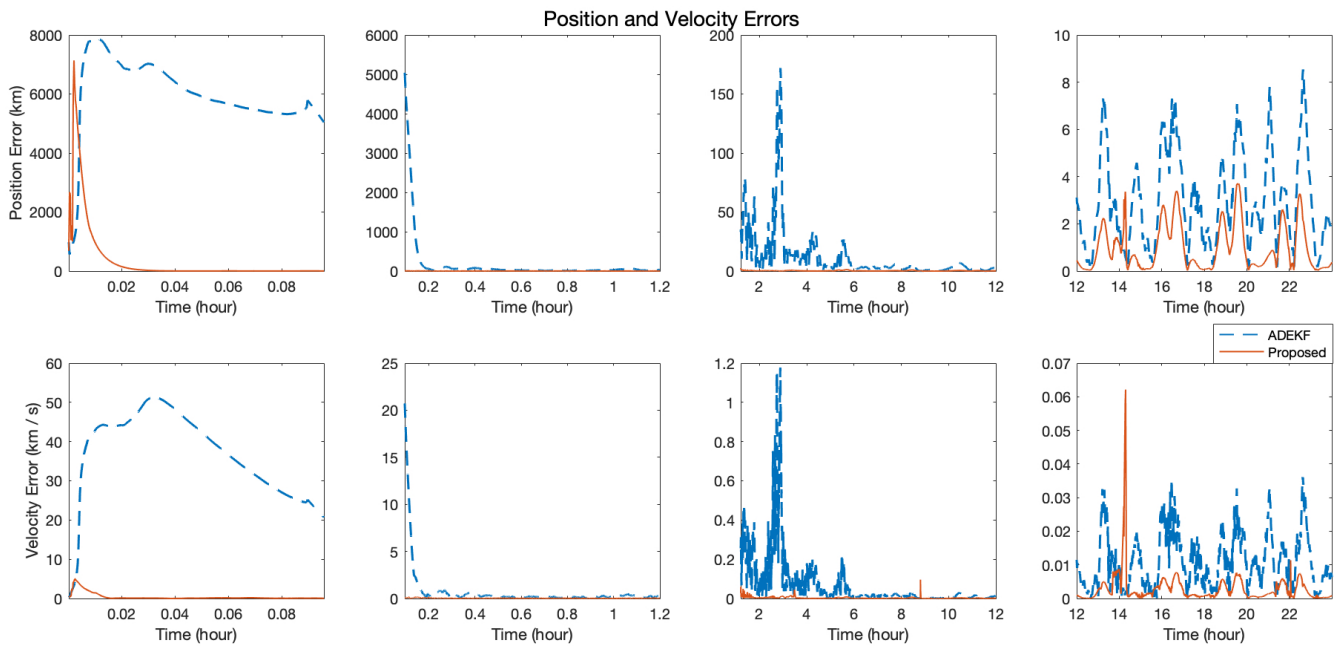


Fig. 6. Position and velocity errors derived from the estimated results.

- 10) Deutschmann, J. K., and Bar-Itzhack, I. Y.: Evaluation of Attitude and Orbit Estimation using Actual Earth Magnetic Field Data, *AIAA J. Guid. Control Dyn.*, **24**, 3, 2001, pp. 616–623.
- 11) Psiaki, M. L., Huang, L., and Fox, S. M.: Ground Tests of Magnetometer-Based Autonomous Navigation (MAGNAV) for Low-Earth-Orbiting Spacecraft, *AIAA J. Guid. Control Dyn.*, **16**, 1, 1993, pp. 206–214.
- 12) Psiaki, M. L.: Autonomous Orbit and Magnetic Field Determination using Magnetometer and Star Sensor Data, *AIAA J. Guid. Control Dyn.*, **18**, 3, 1995, pp. 584–592.
- 13) Psiaki, M. L.: Autonomous Low-Earth-Orbit Determination from Magnetometer and Sun Sensor Data, *AIAA J. Guid. Control Dyn.*, **22**, 2, 1999, pp. 296–304.
- 14) Juang, J. C., Tsai, Y. F., and Tsai, C. T.: Design and Verification of A Magnetometer-Based Orbit Determination and Sensor Calibration Algorithm, *Aerosp. Sci. Tech.*, **21**, 1, 2012, pp. 47–54.
- 15) Cheon, Y. J.: Fast Convergence of Orbit Determination using Geomagnetic Field Measurement in Target Pointing Satellite, *Aerosp. Sci. Tech.*, **30**, 1, 2013, pp. 315–322.
- 16) Wang, X., Zhang, Q., and Li, H.: An Autonomous Navigation Scheme based on Starlight, Geomagnetic and Gyros with Information Fusion for Small Satellites, *Acta Astronaut.*, **94**, 2, 2014, pp. 708–717.
- 17) Ma, H., and Xu, S.: Magnetometer-Only Attitude and Angular Velocity Filtering Estimation for Attitude Changing Spacecraft, *Acta Astronaut.*, **102**, 2014, pp. 89–102.
- 18) H. E. Söken and S.-i. Sakai, “Real-Time Attitude-Independent Magnetometer Bias Estimation for Spinning Spacecraft,” *AIAA J. Guid. Control Dyn.*, pp. 1–4, 2017.
- 19) Wang, M., Wu, W., Wang, J., and Pan, X.: High-Order Attitude Compensation in Coning and Rotation Coexisting Environment, *IEEE Trans. Aerosp. Elect. Syst.*, **51**, 2, 2015, pp. 1178–1190.
- 20) Sun, X., Chen, P., MacAbiau, C., and Han, C.: Autonomous Orbit Determination via Kalman Filtering of Gravity Gradients, *IEEE Trans. Aerosp. Elect. Syst.*, **52**, 5, 2016, pp. 2436–2451.
- 21) Wu, Y., Wang, P., and Hu, X.: Algorithm of Earth-Centered Earth-Fixed Coordinates to Geodetic Coordinates, *IEEE Trans. Aerosp. Elect. Syst.*, **39**, 4, 2003, pp. 1457–1461.
- 22) Zhou, Z., Shen, Y., and Li, B.: A Windowing-Recursive Approach for GPS Real-time Kinematic Positioning, *GPS Solut.*, **14**, 4, 2010, pp. 365–373.
- 23) Zhou, Z., and Li, B.: GNSS Windowing Navigation with Adaptively Constructed Dynamic Model, *GPS Solut.*, **19**, 1, 2014, pp. 37–48.
- 24) Zhou, Z., Li, B., and Shen, Y.: A Window-Recursive Approach for GNSS Kinematic Navigation Using Pseudorange and Doppler Measurements, *J. Navigation*, **66**, 02, 2012, pp. 295–313.

- 25) Olson, W. P., and Pfitzer, K. A., "A Quantitative Model of the Magnetospheric Magnetic Field," *J. Geophysical Res.*, **79**, 25, 1974, pp. 3739–3748.
- 26) Pittelkau, M. E.: Rotation Vector in Attitude Estimation, *AIAA J. Guid. Control Dyn.*, **26**, 6, 2003, pp. 855–860.
- 27) Wu, J.: Optimal Continuous Unit Quaternions from Rotation Matrices, *AIAA J. Guid. Control Dyn.*, **42**, 4, 2019, pp. 919–922.